Performance Enhancement of Low-Cost Land Navigation System for Location-Based Service

Seong Yun Cho and Wan Sik Choi

This work demonstrates a dead-reckoning (DR) scheme for a low-cost land navigation system and a DR/GPS system design using the sigma point Kalman filter (SPKF). Through an observability analysis and some simulations, it is shown that the performances of a stand-alone DR system and DR/GPS system can be improved by employing the proposed DR scheme and SPKF. By using the designed DR scheme and filter, the stand-alone DR system does not have any undetectable errors occurring on the curve trajectory. And the DR/GPS system can provide a stable and seamless navigational solution even in the case where the initial heading estimation error is large, such as 160 degrees, or when the GPS signal is unavailable due to tunnels, buildings, and so on. Simulation results indicate a satisfactory performance of the proposed system.

Keywords: Land navigation, DR/GPS, sigma point Kalman filter.

I. Introduction

Military navigation technology has recently been transformed into core technology for civil navigation. The demand on commercial navigation technology has been increasing for providing location-based service (LBS) such as road guidance, E911 service, surrounding information service, and so on. Generally, LBS has been implemented to serve a driver with a safe and comfortable driving environment.

The navigation system for a driver is called a car navigation system (CNS) and that for a pedestrian is called a personal/pedestrian navigation system (PNS). CNS/PNS can be comprised of a GPS receiver and a digital map. CNS/PNS can be expanded into the integration of a micro-electro-mechanical systems (MEMS)–based dead-reckoning (DR) system and GPS receiver to provide seamless position information even in an urban area where a GPS signal is locally unavailable, such as in a tunnel, near a building, and so on [1]-[5]. A civil navigation system must be implemented with low-cost sensors to extend to a commercial navigation market [6]. Therefore, a DR system must be constructed with a low-cost inertial sensor assembly (ISA) that does not have six degrees of freedom (6DOF). In this paper, a low-cost DR/GPS system is presented, and the DR system is implemented using an accelerometer and two gyros.

In order to calculate a moving distance on the horizontal frame in a DR system, an odometer or accelerometer assembly has been utilized. In general, the DR system for the before market has used an odometer. And the DR system for the after market has utilized an accelerometer assembly. In this paper, a DR system for the after market is considered and a simplified DR scheme is presented. It has been verified that the performance of the presented DR scheme is better than that of

Manuscript received Aug. 22, 2005; revised Nov. 17, 2005.

Seong Yun Cho (phone: + 82 42 869 1636, email: sycho@etri.re.kr) and Wan Sik Choi (email: choiws@etri.re.kr) are with Telematics & USN Research Division, ETRI, Daejeon, Korea.

the conventional DR construction for land navigation. Using the presented DR scheme, the DR/GPS system is more robust to an initial heading estimation error than the conventional DR/GPS system.

Up to now, the DR/GPS system has been developed using the extended Kalman filter (EKF), neural/fuzzy approaches, and some other techniques [2]. The EKF is a well-known approach in the integration of nonlinear systems. However, several flaws of the EKF exist, which may lead to sub-optimal performance and sometimes divergence of the filter [4], [8]. In recent years, the sigma point Kalman filter (SPKF) has been presented and investigated by Julier, Wan, and others to overcome the flaws [9]-[14]. If an initial estimation error is large in the EKF, the filter may diverge because the Jacobian matrix, necessary in the EKF, has serious errors [15]-[17]. The SPKF, however, does not need to calculate the Jacobian matrix. Therefore, it is expected that the SPKF is robust to an initial estimation error, unlike the EKF. In this paper, a performance-enhanced DR/GPS system is designed using the proposed DR scheme and the SPKF.

The performances of the proposed DR scheme and the DR/GPS system using the EKF and SPKF are analyzed in the various situations. The results show that the DR/GPS system using the SPKF works well in various environments such as large initial heading estimation error, GPS signal blockage, and so on.

In the next section, a DR scheme for low-cost land navigation is presented. In section III, a performance-enhanced DR/GPS system is designed using the SPKF. The performance of the proposed DR/GPS system is verified by simulation in section IV. Finally, conclusions are drawn in the last section.

II. A DR Scheme for Low-Cost Land Navigation

The general differential equation for velocity calculation in an Inertial Navigation System (INS) is as follows [4], [5]:

$$\dot{V}^n = C_b^n f^b - (2\omega_{ie}^n + \omega_{en}^n) \times V^n + g^n, \tag{1}$$

where V^n is the velocity on the navigation coordinate, C_b^n is the coordinate transformation matrix from a body-fixed coordinate to navigation coordinate, f^b is the vector of sensed accelerations in a body-fixed coordinate, g^n is the gravity acceleration, and $(2\omega_{ie}^n + \omega_{en}^n) \times V^n$ is the Coriolis force term.

In a two-dimensional case for low-cost land navigation, the Coriolis force term can be ignored. Therefore, the simplified equation for a discrete-time system can be written as

$$V_k^n = V_{k-1}^n + (C_b^n)_k f_k^b d_k + g^n \tag{2}$$

$$P_k^n = P_{k-1}^n + V_k^n d_k, \tag{3}$$

where $V^n = [V_N^n \;\; V_E^n]^T$, $f^b = [f_x^b \;\; f_y^b]^T$, P^n is the position on the navigation coordinate, and d_k is the time interval of the discrete time stamp. This scheme is called DR model1(DRM1) and requires two accelerometers.

Another scheme, DRM2, requiring just an accelerometer, is presented as follows:

$$V_{x,k}^h = V_{x,k-1}^h + f_{x,k}^h d_k \tag{4}$$

$$P_k^n = P_{k-1}^n + \left(C_h^n\right)_k V_{x,k}^h d_k, \tag{5}$$

where V_x^h means the moving axis velocity on the horizontal frame, and f_x^h and C_h^n are as follows:

$$f_{x,k}^h = \left(f_{x,k}^b - g \sin\theta_k\right)\cos\theta_k \tag{6}$$

$$\left(C_h^n\right)_k = \begin{bmatrix} \cos\psi_k \\ \sin\psi_k \end{bmatrix}, \tag{7}$$

where θ and ψ mean the pitch angle and heading angle, respectively.

The sensor configuration used to implement DRM2 is shown in Fig. 1. The sensor module consists of an accelerometer (Accel_x) and two gyros (Gyro_y, Gyro_z). The Accel_x, Gyro_y, and Gyro_z are aligned with the forward axis, the right lateral axis, and the under vertical axis of a vehicle, respectively.

DRM1 updates the velocity on the navigation coordinate by transforming the acceleration on the body-fixed coordinate into that on the navigation coordinate. If the vehicle turns with constant angular velocity (ω) and constant velocity (V), the accelerometers attached on the vehicle output $f^b = [0 \;\; V\omega]^T$. The y-axis (lateral axis) term means the centrifugal force. However, in the case that either the velocity is low or the angular velocity is low, the centrifugal force may not be recognized in the y-axis accelerometer, which is a low-grade MEMS type. This phenomenon may cause a velocity error on the navigation coordinate. Also, the rotary motion of a vehicle cannot be reflected in the position update.

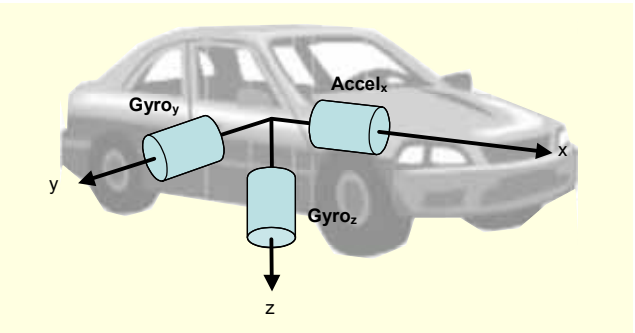

Fig. 1. Sensor construction of the DRM2 system.

DRM2 updates the velocity on the horizontal coordinate using the x-axis accelerometer. The horizontal coordinate is the projected axis of the body-fixed coordinate onto the navigation coordinate. Unless a vehicle slips, the vehicle moves only to the direction of the x-axis (longitudinal axis). And the output of the x-axis accelerometer does not contain the centrifugal force on the curve trajectory because the x-axis vector is parallel to the tangential vector of the curve. Therefore, the rotary motion of a vehicle is surely reflected in the position update just using the heading angle calculated by a z-axis gyro.

The performance difference between the two methods also appeared in the DR/GPS integration. In order to analyze the performances of the two methods, the DR/GPS integration is simulated using the EKF. Figure 2 shows the gyro bias covariance. The gyro bias in the DRM2/GPS is observable irrespective of the trajectory because the gyro bias covariance decreases with time. However, the observability of the DRM1/GPS varies according to the moving trajectory. As can be seen in Fig. 2, the gyro bias covariance in the DRM1/GPS decreases rapidly on the turning section. This phenomenon means that the gyro bias can be estimated just on the curve trajectory. Therefore, the estimation performance of the DRM2/GPS is better than that of the DRM1/GPS.

Figure 3 shows the heading error according to the initial azimuth estimation error. The initial heading error is 45° in Figs. 3(a) and 3(c), and is 90° in Figs. 3(b) and 3(d). The vehicle turns by 20°/s for 15 to 25 s in Figs. 3(a) and 3(b), and for 15 to 53 s in Figs. 3(c) and 3(e). It can be seen that the heading error in the DRM2/GPS converges into 0 even in the case where the initial heading estimation error is large. However, the convergence of the heading error in the DRM1/GPS is dependent on the moving trajectory and the initial estimation error size. Therefore, it is confirmed that the DRM2/GPS has better performance than the DRM1/GPS.

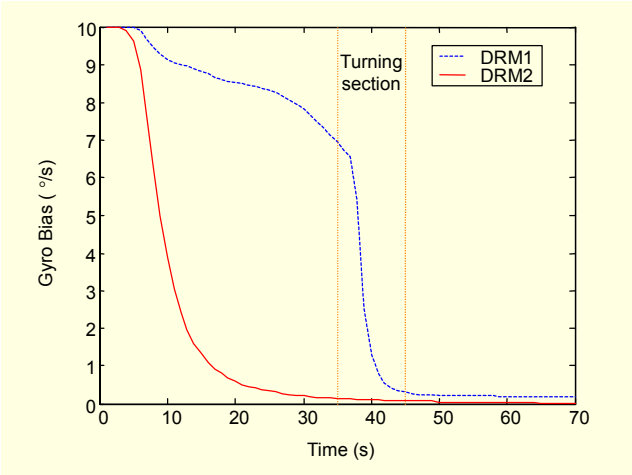

Fig. 2. Gyro bias covariance.

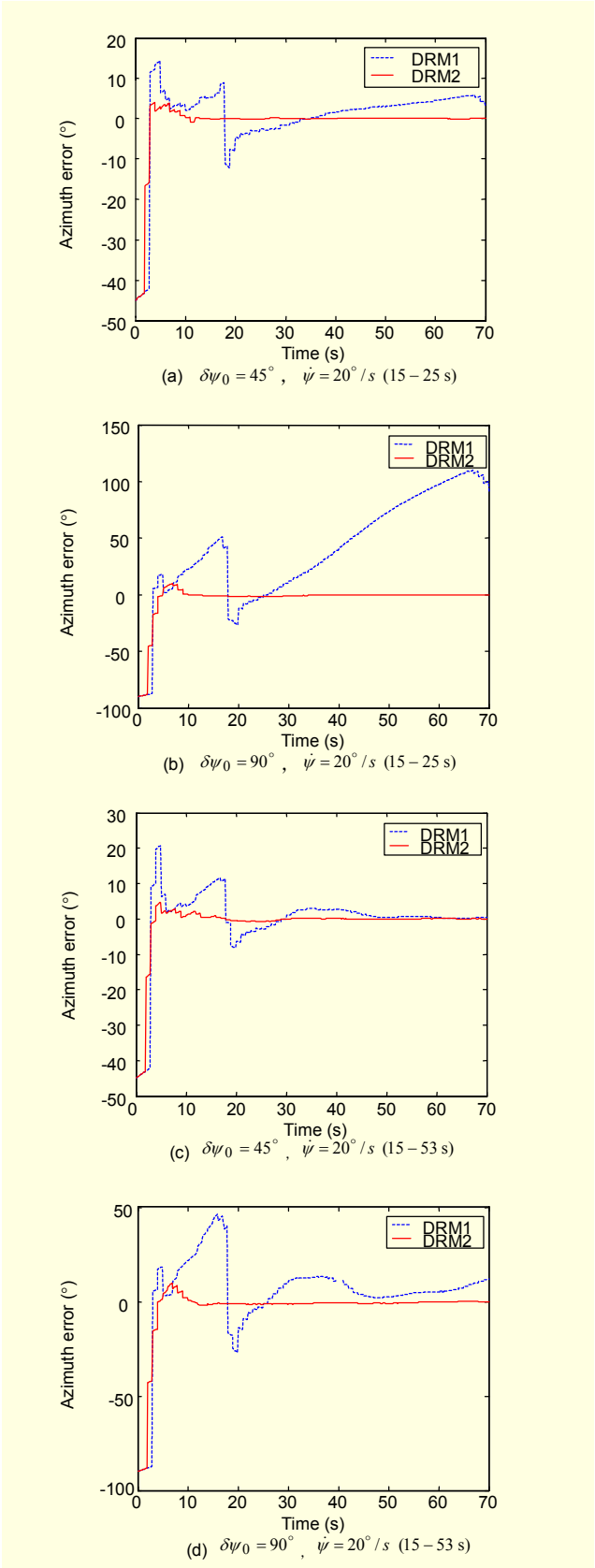

Fig. 3. Performance comparison between DRM1 and DRM2 in DR/GPS integration according to the initial heading error.

III. Performance Enhanced Low-Cost DR/GPS System

The CNS for location-based service must provide a navigation solution seamlessly, and a DR/GPS system can be adopted. In a DR/GPS system, it is important to choose a proper integration filter. In this paper, the sigma point Kalman filter is utilized. It is also important to consider the state variables in filter design. The state variables must be selected to satisfy full observability. In this paper, state variables are first selected with

$$x_1 = \begin{bmatrix} P_N^n & P_E^n & V_x^h & \theta & \psi \end{bmatrix}^T, \tag{8}$$

where P_N^n, P_E^n is the two-dimensional position on the navigation coordinate, V_x^h is the moving velocity on the horizontal coordinate, θ is the pitch angle, and ψ is the heading angle.

Then, the sensor error is considered. Generally, the errors for low-cost sensors can be modeled as follows:

$$\tilde{f}_x^b = \left(SF_{ax} + \delta_{ax}\right)\left(f_x^b + \nabla_x\right) \tag{9}$$

$$\tilde{\omega}_y^b = \left(SF_{gy} + \delta_{gy}\right)\left(\omega_y^b + \varepsilon_y\right), \tag{10}$$

where ∇_x denotes the bias of the x-axis accelerometer, δ_{ax} means the scale factor error of the accelerometer, ε_y denotes the bias of the y-axis gyro, and δ_{gy} indicates the scale factor error of the gyro.

In this case, the moving axis acceleration on the horizontal frame, (6), can be estimated as follows:

$$\begin{aligned} \hat{f}_{x,k}^h = & \left(SF_{ax} + \delta_{ax,k} - \hat{\delta}_{ax,k}\right) \\ & \times \left(f_{x,k}^b + \nabla_{x,k} - \hat{\nabla}_{x,k} - g\sin(\theta_k + \delta\theta_k - \delta\hat{\theta}_k)\right) \\ & \times \cos(\theta_k + \delta\theta_k - \delta\hat{\theta}_k) d_k, \end{aligned} \tag{11}$$

where $\hat{\nabla}_x$, $\hat{\delta}_{ax}$, and $\delta\hat{\theta}$ denote the estimated bias, estimated scale factor error, and estimated pitch error, respectively.

As can be seen in this equation, the accelerometer bias and pitch error are coupled in a bracket. If a filter estimates all of the errors, it can be anticipated that the filter may not have full observability. Figure 4 shows the estimation property according to the accelerometer error model. In this figure, model 1 means that the accelerometer error is modeled as (8), and model 2 denotes that the accelerometer error is modeled simply as the scale factor error.

$$\tilde{f}_x^b = \left(SF_{ax} + \delta_{ax}\right) f_x^b \tag{12}$$

$$\tilde{\omega}_y^b = \left(SF_{gy} + \delta_{gy}\right) \omega_y^b, \tag{13}$$

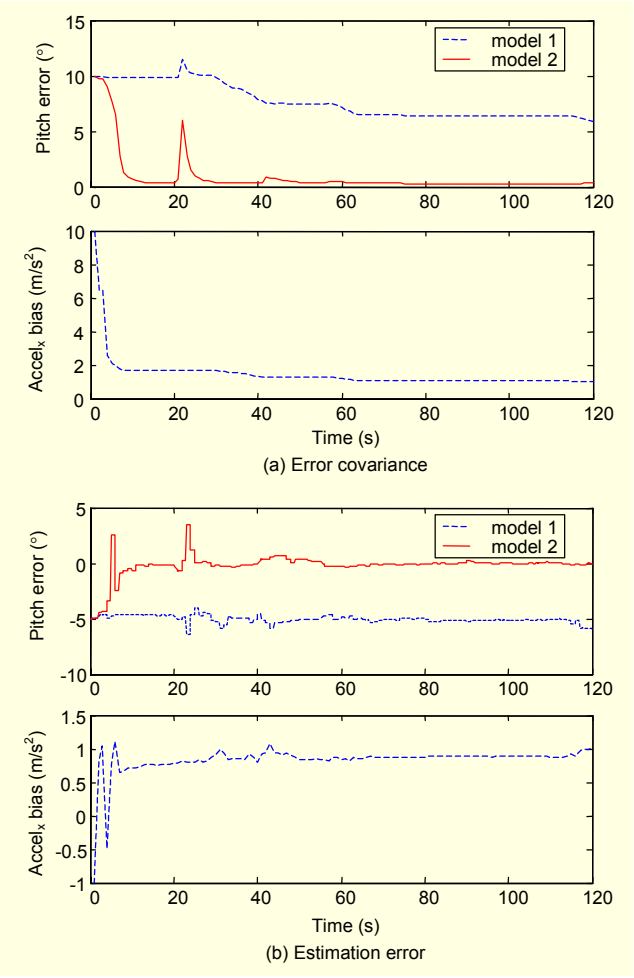

Fig. 4. Estimation property according to the accelerometer error model.

where ω_y^b is the y-axis gyro output.

The state vectors for the simulation are as follows:

$$x_{model1} = \begin{bmatrix} x_1^T & \vdots & \nabla_x & \varepsilon_y & \varepsilon_z & \delta_{ax} & \delta_{gy} & \delta_{gz} \end{bmatrix}^T, \tag{14a}$$

$$x_{model2} = \begin{bmatrix} x_1^T & \vdots & \delta_{ax} & \delta_{gy} & \delta_{gz} \end{bmatrix}^T. \tag{14b}$$

As estimated previously, the pitch error and the accelerometer bias of the filter with model 1 are not observable. The estimated pitch and accelerometer bias have large errors. On the other hand, the pitch error of the filter with model 2 is observable. As can be seen in Fig. 4, the pitch error is estimated accurately. Therefore, the accelerometer error is modeled as model 2, in this paper. The gyro error is modeled as the scale factor error, also. The bias of a gyro can be calibrated during the standing phase.

If the DR system is integrated with a GPS receiver using the EKF, a linearized equation containing a Jacobian matrix must be derived. The error state vector in the EKF is as follows:

$$\delta x = \begin{bmatrix} \delta P_N^n & \delta P_E^n & \delta V_x^h & \delta\theta & \delta\psi & \delta_{ax} & \delta_{gy} & \delta_{gz} \end{bmatrix}^T \quad (15)$$

where $(\delta P_N^n, \delta P_E^n)$ is the two-dimensional position error on the navigation coordinate, δV_x^h is the moving velocity error on the horizontal coordinate, $\delta\theta$ is the pitch angle error, $\delta\psi$ is the heading angle error, δ_{ax} is the accelerometer scale factor error, and δ_{gy}, δ_{gz} are the gyro scale factor errors.

The linearized equation for the discrete-time system is derived as follows (see the appendix for more details):

$$\begin{aligned} x_k &= \begin{bmatrix} I_{2\times2} & A_1\Delta t & A_2\Delta t & 0_{2\times1} & 0_{2\times2} \\ 0_{1\times2} & 1 & A_3\Delta t & SF_{ax} f_{x,k}^b \cos\theta_k \Delta t & 0_{1\times2} \\ 0_{2\times2} & 0_{2\times1} & I_{2\times2} & 0_{2\times1} & A_4\Delta t \\ 0_{1\times2} & 0 & 0_{1\times2} & 1 & 0_{1\times2} \\ 0_{2\times2} & 0_{2\times1} & 0_{2\times2} & 0_{2\times1} & I_{2\times2} \end{bmatrix} x_{k-1} \\ &\quad + w_k, \qquad w_k \sim N(0, Q) \\ y_k &= \begin{bmatrix} I_{3\times3} & 0_{3\times5} \end{bmatrix} x_k + v_k, \quad v_k \sim N(0, R), \end{aligned} \quad (16)$$

where Δt is the step size for filter update, and

$$A_1 = \begin{bmatrix} \cos\psi_k \\ \sin\psi_k \end{bmatrix}, \quad (17a)$$

$$A_2 = \begin{bmatrix} 0 & -V_{x,k}^h \sin\psi_k \\ 0 & V_{x,k}^h \cos\psi_k \end{bmatrix}, \quad (17b)$$

$$A_3 = \begin{bmatrix} g\sin^2\theta_k - SF_{ax} f_{x,k}^b \sin\theta_k - g\cos^2\theta_k & 0 \end{bmatrix}, \quad (17c)$$

$$A_4 = \begin{bmatrix} \omega_{y,k}^b & 0 \\ 0 & \omega_{z,k}^b \end{bmatrix}. \quad (17d)$$

In a low-cost DR/GPS system, a tightly coupled integration is impossible because recent low-cost GPS receivers do not provide raw data such as satellite position, pseudorange, and so on. In a loosely coupled DR/GPS system, the measurement can be set by position error and velocity error as follows:

$$z_k = \begin{bmatrix} P_{N,k}^h \\ P_{E,k}^h \\ V_{x,k}^h \end{bmatrix} - \begin{bmatrix} \left(P_{Lat,k}^{GPS} - P_{Lat,0}^{GPS}\right) R_e \\ \left(P_{Lon,k}^{GPS} - P_{Lon,0}^{GPS}\right) R_e \cos(P_{Lat,k}^{GPS}) \\ \sqrt{\left(V_{Lat,k}^{GPS}\right)^2 + \left(V_{Lon,k}^{GPS}\right)^2} \end{bmatrix}. \quad (18)$$

where P^h is the position on the horizontal coordinate calculated by DR, $P_{Lat/Lon}^{GPS}$ is the position (latitude/longitude) calculated by GPS, and R_e is the radius of the earth.

In this paper, the DR system is integrated with a GPS receiver using the SPKF to compare the efficiency of the EKF and the SPKF, and to analyze the performance of the proposed DR scheme.

The optimal solution of the state estimation in a nonlinear system can be obtained by the recursive Bayesian estimator. However, the implementation of a high-order system is difficult. An approximation approach for implementing a real system is the EKF. Unfortunately, the EKF suffers a well-known problem: Jacobian matrices to linearize the nonlinear system/measurement matrices. This weak point can be overcome by the particle filter that uses a finite set of samples from an assumed probability distribution and then transforms each sample independently with an expectation that the collective statistics of the ensemble set of samples will accurately reflect the statistics of the evolving system of interest. Although the particle filter avoids some difficulties, the number of samples required to achieve reliable estimates must be large (for example, many thousands in a two or three dimension). This may lead to an implementation problem. An additional mechanism, a re-sampling technique, has been developed to overcome this problem. However, the particle filter still has a tradeoff between the computational burden and reliability. Recently, an unscented transformation (UT) concept has been developed to solve the drawbacks of the EKF and the particle filter. The UT approximates the Gaussian distribution using a small number of samples, referred to as sigma points. A sigma point Kalman filter (SPKF) is a special type of Kalman filter constructed using the UT concept. The SPKF can be implemented in several different forms such as the unscented Kalman filter, central difference Kalman filter, square-root unscented Kalman filter, square-root central difference Kalman filter, reduced sigma point filter, and so on [7]-[13].

Generally, the number of sigma points is $2L+1$ (augmented state dimension L). However, in the reduced sigma point filter, a set of $L+2$ sigma points can be constructed that fully captures all of the known statistics of the distribution. There are several types of UT in the reduced sigma point filter such as the spherical simplex UT, the scaled UT, and so on. In this paper the scaled UT is utilized to implement the SPKF [10].

First, the augmented states and covariance matrix are initialized:

$$\hat{x}_0^a = E\begin{bmatrix} x_0^T & v_0 \end{bmatrix}^T = \begin{bmatrix} \hat{x}_0^T & 0 \end{bmatrix}^T \quad (19)$$

$$P_0^a = E\left[\left(x_0 - \hat{x}_0^a\right)\left(x_0 - \hat{x}_0^a\right)^T\right] = \begin{bmatrix} P_0 & 0 \\ 0 & Q \end{bmatrix}, \quad (20)$$

where P_0 is the initial error covariance matrix, and Q is the process noise covariance matrix.

Then, weights factors are also initialized.

$$W_0^{(m)} = \left(w_0 - 1\right)/\alpha^2 + 1 \quad (21a)$$

$$W_0^{(c)} = (w_0 - 1)/\alpha^2 + 2 + \beta - \alpha^2 \tag{21b}$$

$$w_i = (1 - w_0)/(L+1), \; i = 1, \cdots, L+1 \tag{21c}$$

$$W_i^{(m)} = W_i^{(c)} = w_i / \alpha^2 , \tag{21d}$$

where $10^{-4} \le \alpha \le 1$ and $0 \le w_0 \le 1$ are scaling parameters, and β is a parameter to minimize higher order effects; this term is minimized when $\beta = 2$ [9].

After initialization, sigma points are calculated using the assumed probability distribution.

$$\chi_{k-1}^a = 0_{L\times(L+2)} \tag{22a}$$

$$\chi_{k-1}^a(i, 2:i+1) = \frac{-1}{\sqrt{i(i+1)w_1}} \tag{22b}$$

$$\chi_{k-1}^a(i, i+2) = \frac{i}{\sqrt{i(i+1)w_1}} \tag{22c}$$

$$\chi_{k-1}^a(1:L,\ j) = \hat{x}_{k-1}^a + \alpha S^T \chi_{k-1}^a(1:L,\ j) , \tag{22d}$$

where i=1,…, L and j=1,…, L+2.

The matrix S in (22d) can be obtained using Cholesky decomposition as follows:

$$S^T S = P^a. \tag{23}$$

Each sigma point is transformed using the nonlinear system function independently.

$$\chi_{k|k-1}^x(1, j) = \chi_{k-1}^x(1, j) + \chi_{k-1}^x(3, j)\cos\left(\chi_{k-1}^x(5, j)\right)d_k + \chi_{k-1}^w(1, j) \tag{24a}$$

$$\chi_{k|k-1}^x(2, j) = \chi_{k-1}^x(2, j) + \chi_{k-1}^x(3, j)\sin\left(\chi_{k-1}^x(5, j)\right)d_k + \chi_{k-1}^w(2, j) \tag{24b}$$

$$\chi_{k|k-1}^x(3, j) = \chi_{k-1}^x(3, j) + \left(SF_{ax} - \chi_{k-1}^x(6, j)\right) \times \left(f_x^b - g\sin\left(\chi_{k-1}^x(4, j)\right)\right)\cos\left(\chi_{k-1}^x(4, j)\right)d_k + \chi_{k-1}^w(3, j) \tag{24c}$$

$$\chi_{k|k-1}^x(4, j) = \chi_{k-1}^x(4, j) + \left(SF_{gy} - \chi_{k-1}^x(7, j)\right)\omega_y d_k + \chi_{k-1}^w(4, j) \tag{24d}$$

$$\chi_{k|k-1}^x(5, j) = \chi_{k-1}^x(5, j) + \left(SF_{gz} - \chi_{k-1}^x(8, j)\right)\omega_z d_k + \chi_{k-1}^w(5, j) \tag{24e}$$

$$\chi_{k|k-1}^x(6, j) = \chi_{k-1}^x(6, j) + \chi_{k-1}^w(6, j) \tag{24f}$$

$$\chi_{k|k-1}^x(7, j) = \chi_{k-1}^x(7, j) + \chi_{k-1}^w(7, j) \tag{24g}$$

$$\chi_{k|k-1}^x(8, j) = \chi_{k-1}^x(8, j) + \chi_{k-1}^w(8, j) , \tag{24h}$$

where $j = 1, \cdots, L+2$,

$\chi^x(1,j)$ is the north-axis position on the horizontal coordinate,

$\chi^x(2,j)$ is the east-axis position on the horizontal coordinate,

$\chi^x(3,j)$ is the forward velocity of a vehicle on the horizontal coordinate,

$\chi^x(4,j)$ is the pitch angle,

$\chi^x(5,j)$ is the heading angle,

$\chi^x(6,j)$ is the accelerometer scale factor,

$\chi^x(7,j)$ is the y-axis gyro scale factor, and

$\chi^x(8,j)$ is the z-axis gyro scale factor.

State time propagation is completed using the transformed sigma points as follows:

$$\hat{x}_k^- = \sum_{i=0}^{L+1} W_i^{(m)} \chi_{k|k-1}^x(1:L,\ i) . \tag{25}$$

In this paper, it is assumed that the DR system calculates a navigation solution at 10 Hz, and a GPS receiver provides a navigation solution at 1 Hz. Therefore, the state time propagation is processed at 10 Hz. When GPS data is generated, time propagation of the error covariance and the measurement is completed as follows:

$$P_k^- = \sum_{i=0}^{L+1} W_i^{(c)} \left[\chi_{k|k-1}^x(1:L, i) - \hat{x}_k^-\right]\left[\chi_{k|k-1}^x(1:L, i) - \hat{x}_k^-\right]^T \tag{26}$$

$$\hat{y}_k^- = \sum_{i=0}^{L+1} W_i^{(m)} \chi_{k|k-1}^x(1:3,\ i) . \tag{27}$$

Then, a measurement update process is carried out:

$$\hat{x}_k = \hat{x}_k^- + K_k\left(y_k - \hat{y}_k^-\right) \tag{28}$$

$$P_k = P_k^- - K_k P_{y_k y_k} K_k^T , \tag{29}$$

where

$$P_{y_k y_k} = \sum_{i=0}^{L+1} W_i^{(c)} \left[h\left(\chi_{k|k-1}^x(1:L, i)\right) - \hat{y}_k^-\right]\left[h\left(\chi_{k|k-1}^x(1:L, i)\right) - \hat{y}_k^-\right]^T \tag{30}$$

$$P_{x_k y_k} = \sum_{i=0}^{L+1} W_i^{(c)} \left[\chi_{k|k-1}^x(1:L, i) - \hat{x}_k^-\right]\left[h\left(\chi_{k|k-1}^x(1:L, i)\right) - \hat{y}_k^-\right]^T \tag{31}$$

$$K_k = P_{x_k y_k} P_{y_k y_k}^{-1} . \tag{32}$$

The SPKF is processed using (22d) through (32), recursively.

Figure 5 shows the block diagram of the loosely coupled DR/GPS system using the SPKF.

It is a well-known fact that the SPKF can overcome the flaws of the EKF such as an inaccurate Jacobian matrix caused by the linear approximation of a nonlinear function with large initial estimation error. Therefore, it can be expected that the SPKF can drive the DR/GPS system even if the estimated initial heading error is large.

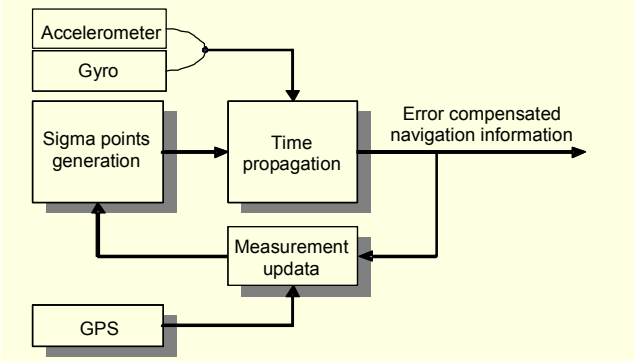

Fig. 5. A block diagram of the loosely coupled DR/GPS system using the SPKF.

IV. Simulation and Experimental Results

In order to verify the performances of the proposed DR scheme and DR/GPS system using the SPKF, a simulation and experiment are carried out.

1. Simulation

Three situations are made in which the EKF and SPKF are driven. Then, the performances of these filters are analyzed. Simulation trajectory includes acceleration/deceleration, uniform motion, rotation, and slope changes as in Fig. 6. GPS data is generated using MATLAB Toolbox. It is assumed that GPS data contains thermal noise, a tropospheric error, and multipath error. In this work, an initial error covariance matrix P_0, process noise covariance matrix Q, and measurement noise covariance matrix R for a filter are chosen. And they are

$$P_0 = \mathrm{diag}\{(50\,\mathrm{m})^2 \quad (50\,\mathrm{m})^2 \quad (5\,\mathrm{m/s})^2 \quad (10^\circ)^2 \quad (180^\circ)^2 \quad (1)^2 \quad (1)^2 \quad (1)^2\} \tag{33}$$

$$Q = \mathrm{diag}\{0 \quad 0 \quad (0.1\ \mathrm{m/s^2})^2 \quad (0.1^\circ)^2 \quad (0.1^\circ)^2 \quad 0 \quad 0 \quad 0\} \tag{34}$$

$$R = \mathrm{diag}\{(15\,\mathrm{m})^2 \quad (15\,\mathrm{m})^2 \quad (0.3\,\mathrm{m/s})^2\}. \tag{35}$$

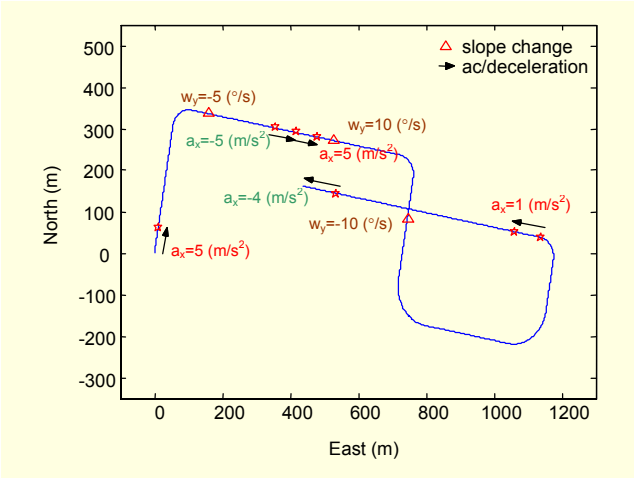

Fig. 6. Simulation trajectory.

A. Situation I

In general, sensor errors in a DR system are expressed as a random constant or a random walk. In this situation, the scale factor errors of the inertial sensors are considered as zero-mean stationary and are modeled as a random constant. It is assumed that the initial estimation errors of the pitch and heading angles are -5 degrees and -10 degrees, respectively. The normalized scale factor errors are set by

$$[\delta_{ax} \quad \delta_{gy} \quad \delta_{gz}] = [0.2 \quad 0.1 \quad -0.1]\,. \tag{36}$$

Figure 7 shows the results of the DR/GPS integration in situation I. The scale factor error of the z-axis gyro in the SPKF is estimated faster than that in the EKF, as shown in Fig. 7(d). This phenomenon causes the larger heading error in the EKF than in the SPKF, as shown in Fig. 7(b). The estimation error of the accelerometer scale factor error in the SPKF decreases slowly, as shown in Fig. 7(c), because the estimation error covariance in the SPKF is slightly larger than that in the EKF in the initial section of movement, as shown in Fig. 7(e).

The position error in the EKF is larger than that in the SPKF. In particular, the position error in the EKF increases on the curve trajectory, as shown in Fig. 7(a), because this error is related with the heading estimation error.

The GPS position error is bounded. However, the output rate is 1 Hz and the position data is scattered within a limit. On the other hand, the position in the SPKF is smooth. In this result, it can be expected that the SPKF has better performance than the EKF.

B. Situation II

The initial heading information cannot be obtained unless a magnetic compass or a high-grade gyro module is utilized.

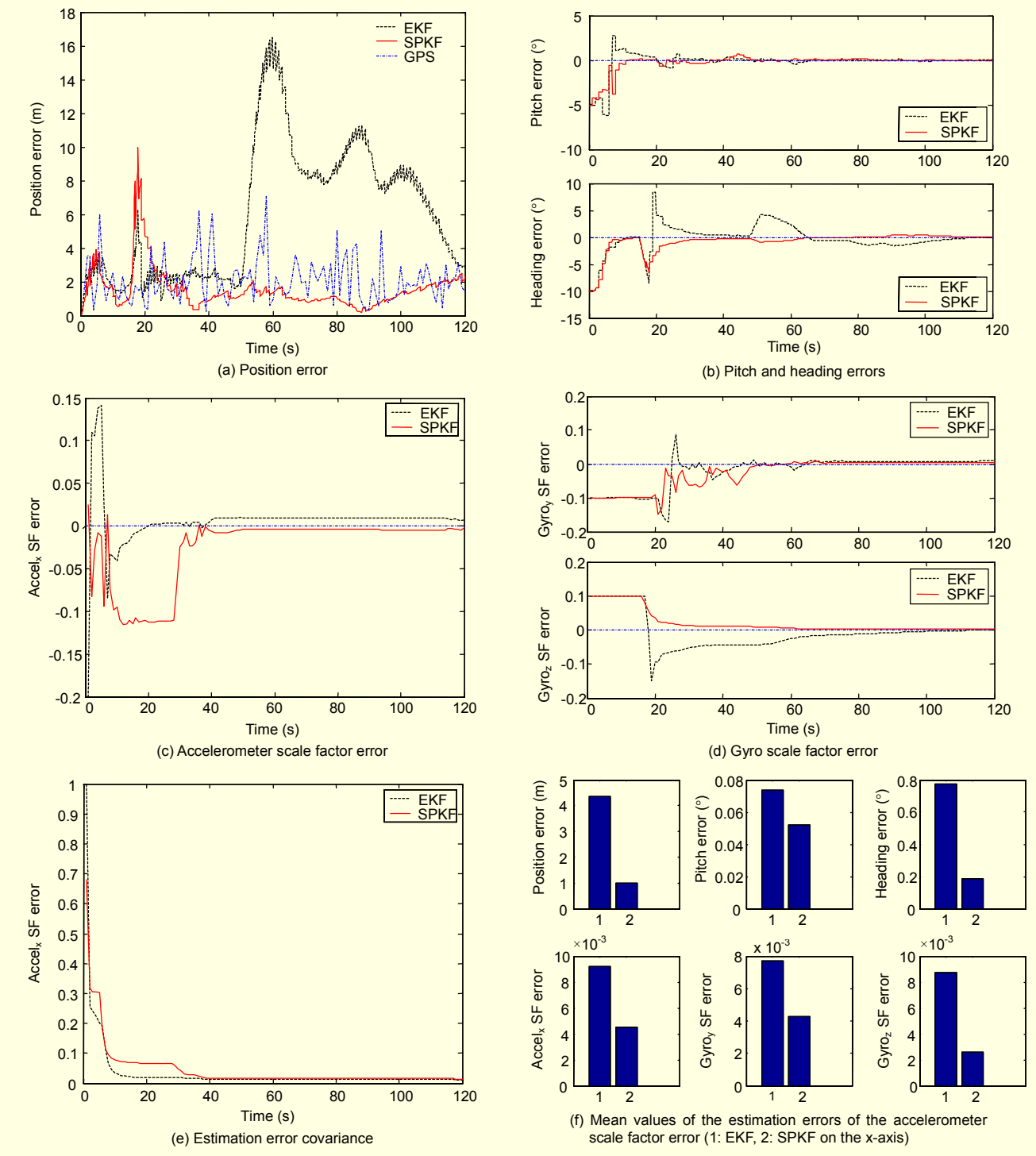

Fig. 7. Results of situation I.

Therefore, the initial heading error exists unavoidably. In this situation, the initial heading error is set by -140 degrees.

Figure 8 shows the simulation results. As can be seen in this figure, the EKF errors diverge with time. On the other hand, the errors of SPKF converge to the neighbor of 0 with time. This phenomenon is owing to the Jacobian matrix error. The SPKF need not calculate the Jacobian matrix. Therefore, the DR/GPS system using the SPKF is robust to the initial large estimation error. However, the DR/GPS system using the EKF also has a good performance if the initial heading estimation error is less than 100 degrees because of the proposed DR scheme.

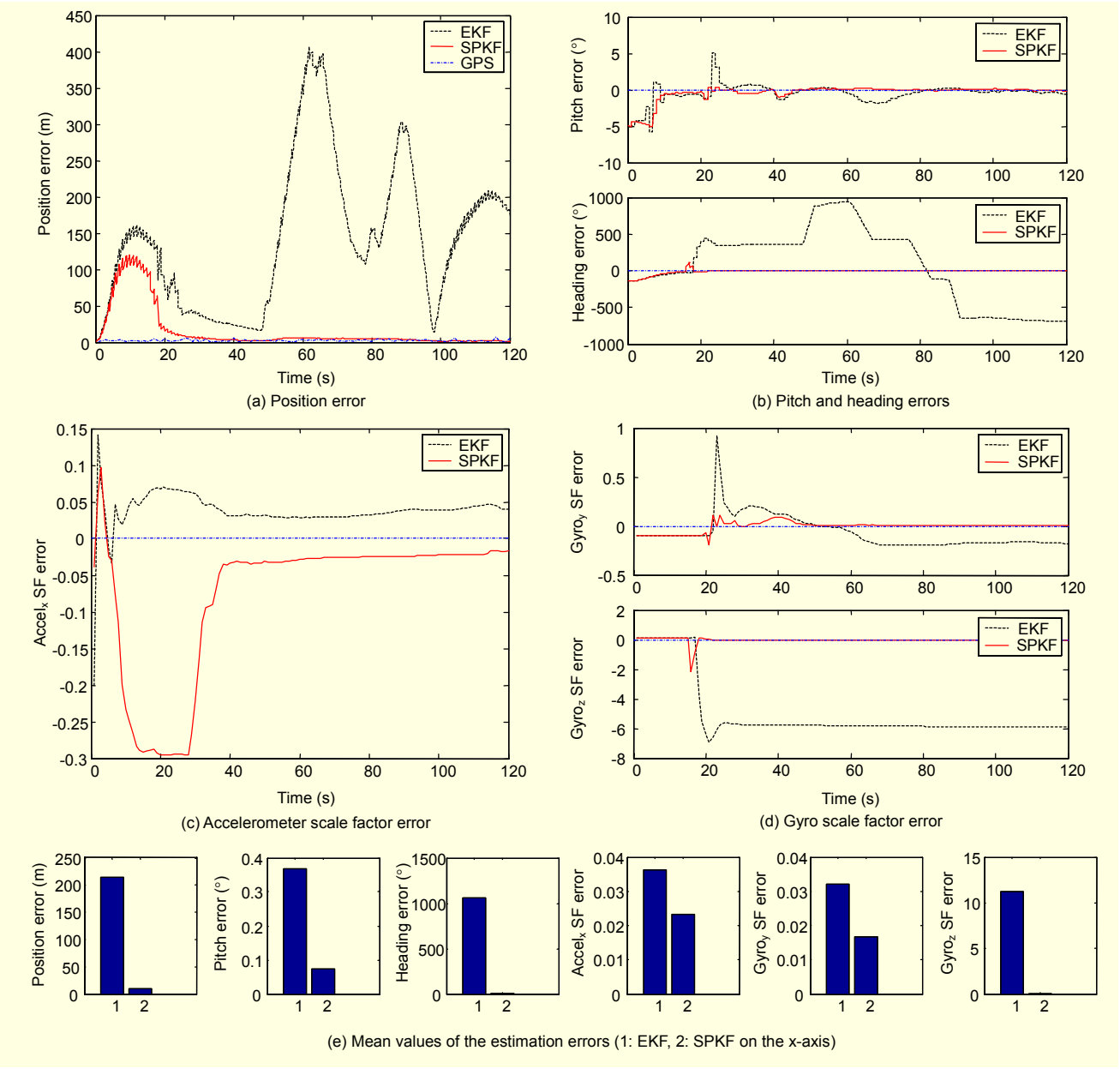

Fig. 8. Results of situation II.

C. Situation III

In this situation, a vehicle with the DR/GPS system passes through a tunnel. Therefore, the GPS signal is blocked and the integration filter cannot process the measurement update in this time section [75, 90]. In this section, only the time propagation process is carried out. It can be seen from Fig. 9 that the SPKF can estimate the sensor errors better than the EKF before the blockage section. Therefore, the position and heading errors of the EKF increase more than that of the SPKF in the blockage section.

From these simulations, it can be expected that the DR/GPS with the SPKF is more robust to various error environments than that with the EKF.

2. Experiment

A. Experiment Description

The trajectory used for experiment on the adopted DR scheme and DR/GPS system was carried out for a moving van using two GPS receivers and an inertial sensor module. The experimental setup is shown in Fig. 10. A reference positioning system was implemented using the DGPS scheme. The antennae of the rover system were attached to a frame mounted on the roof of the van. The data set was collected in Daejeon,

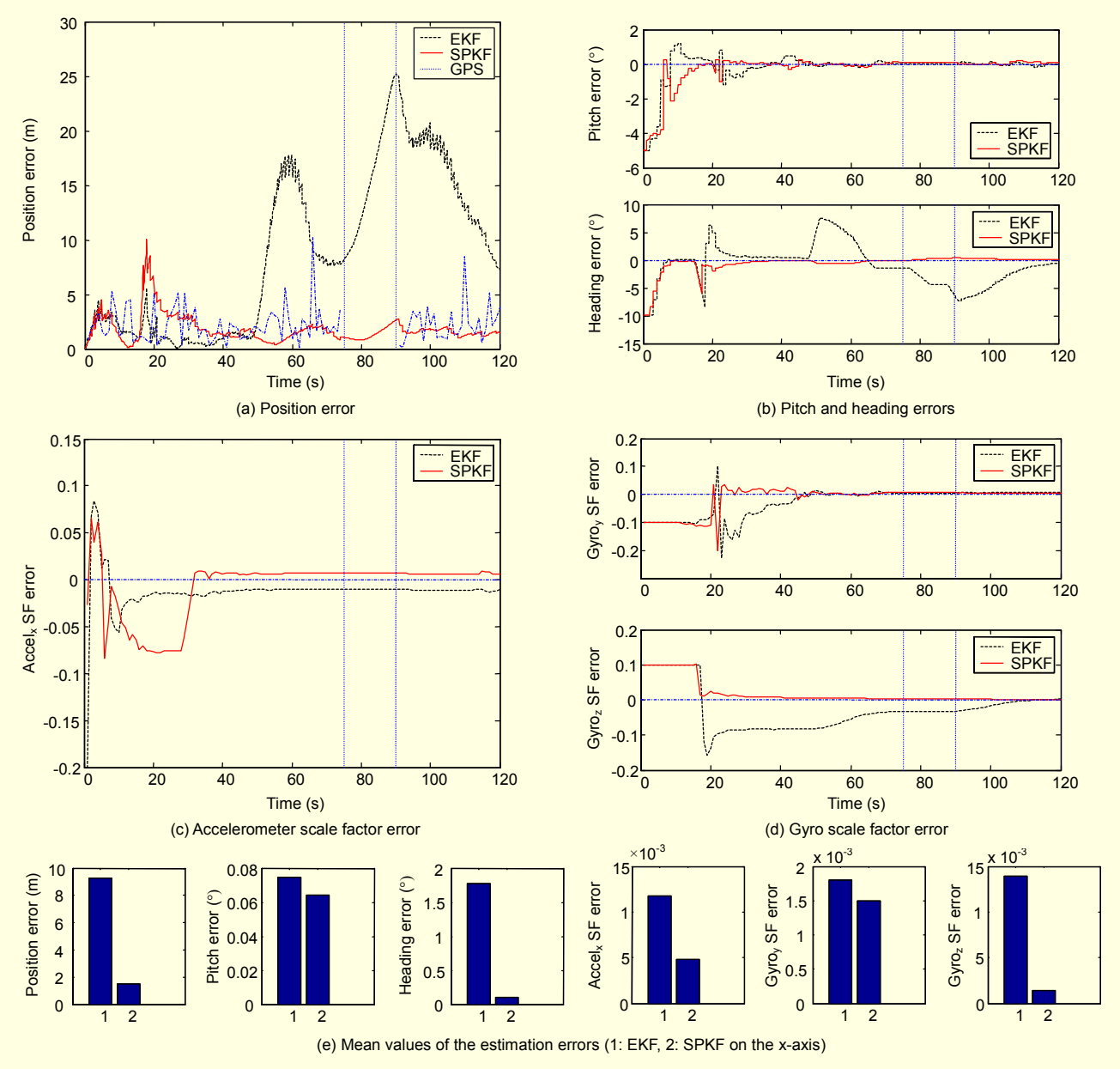

Fig. 9. Results of situation III.

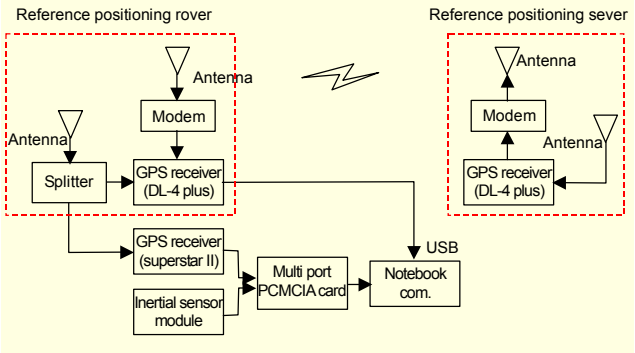

Fig. 10. Experimental setup.

Korea using NovAtel DL-4 plus GPS receiver, Superstar II GPS receiver, and Crossbow DMU-300cc inertial sensor module. The van test trajectory is shown in Fig. 11(a). As can be seen in Fig. 11(b), the number of visible satellites is 0 in section (A). The matched position section is shown in Fig. 11(a), $[\Delta \nabla]$. Figure 11(c) shows the heading angle calculated by the GPS receiver. Sections (B), (C), and (D) indicate the stationary condition. The value of (D) was utilized as reference heading information.

B. Experimental Results

The collected sensor data were processed: first pure DR, then

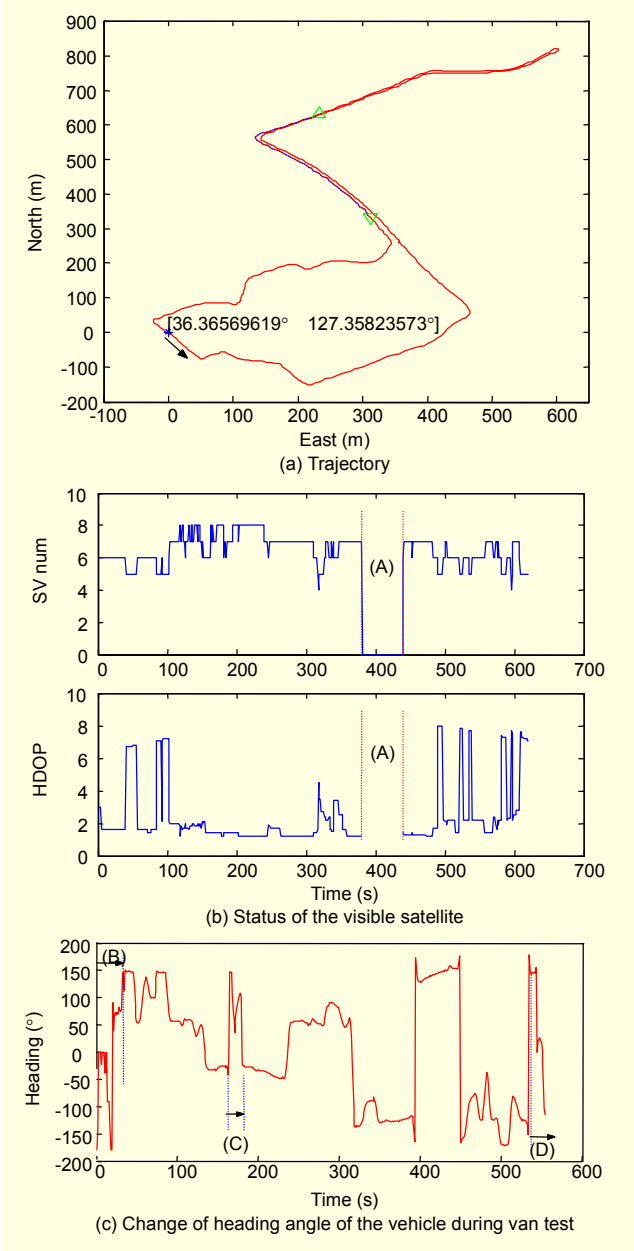

Fig. 11. Trajectory information.

DR/GPS integration using EKF and SPKF. In the former case, a performance comparison between DRM1 and DRM2 was carried out. In the latter case, the performance of the SPKF was compared with the EKF.

Figure 12 shows the results of pure DR processing. Figure 12(a) is the calculated position using DRM1, and Figure 12 is the computed position using DRM2. By comparing with Fig. 11(a), only Fig. 12(b) has a similar trajectory pattern. The reason is that DRM1 containing low-grade accelerometers may not detect the centrifugal force on the curve trajectory and this causes a serious position error. However, DRM2 does not have to detect the centrifugal force. It can be seen that the position and attitude have accumulating errors with time. These errors can be compensated in the DR/GPS integration.

Figures 13 and 14 are the results of the DR/GPS using the EKF and SPKF, respectively. In this case, the DR was implemented using DRM2. It was assumed that the initial estimated heading angle is 70 degrees (the initial heading angle is about 140 degrees). In the position figures, the dotted line indicates the true trajectory, and the solid line indicates the estimated position data. As can be seen in this figure, the erroneous initial heading angle is converged into the right heading angle because of the DR scheme. The pitch angle error is bounded and the motion of the vehicle is reflected. In the GPS signal blockage, however, the velocity increases in spite of the steady velocity of the vehicle when the integration filter is the EKF. This error causes a large position error as can be seen in Fig. 13(a). On the other hand, the velocity remains steady in the GPS signal blockage when the SPKF is utilized. Moreover, the position solution has a small error in this section. It can be deduced that the estimation error of the sensor error in the SPKF is less than that in the EKF. Therefore, the performance of the pure DR in the GPS signal blockage can be maintained in the SPKF case.

In the velocity figures, it can be seen that the calculated velocity is zero when the vehicle is stationary, indicated by the arrowed sections. This can be achieved by a zero-velocity

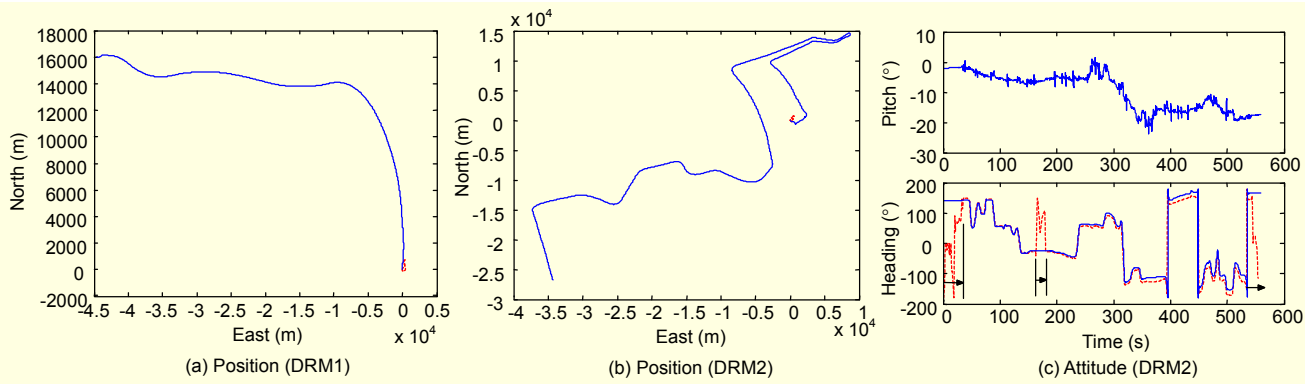

Fig. 12. Results of pure DR processing.

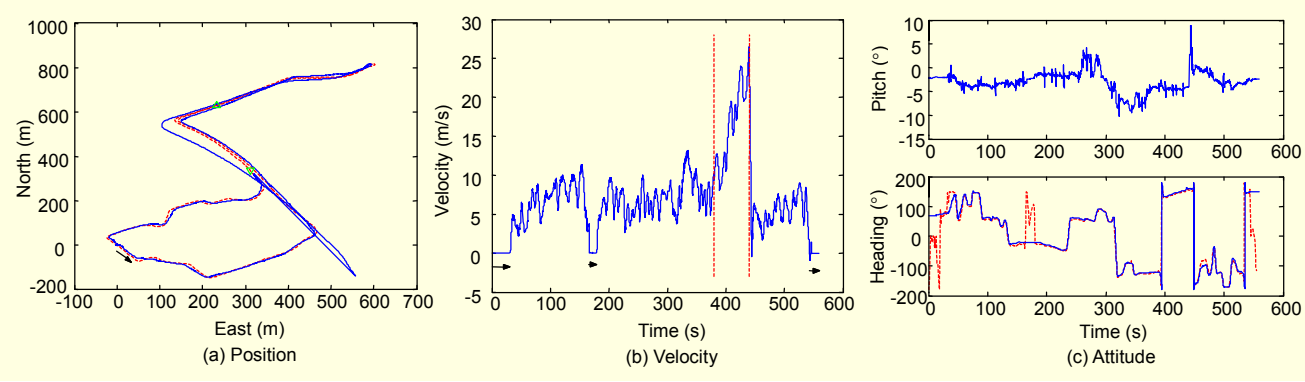

Fig. 13. Results of the DR/GPS using the EKF (initial estimated heading angle is 70 °).

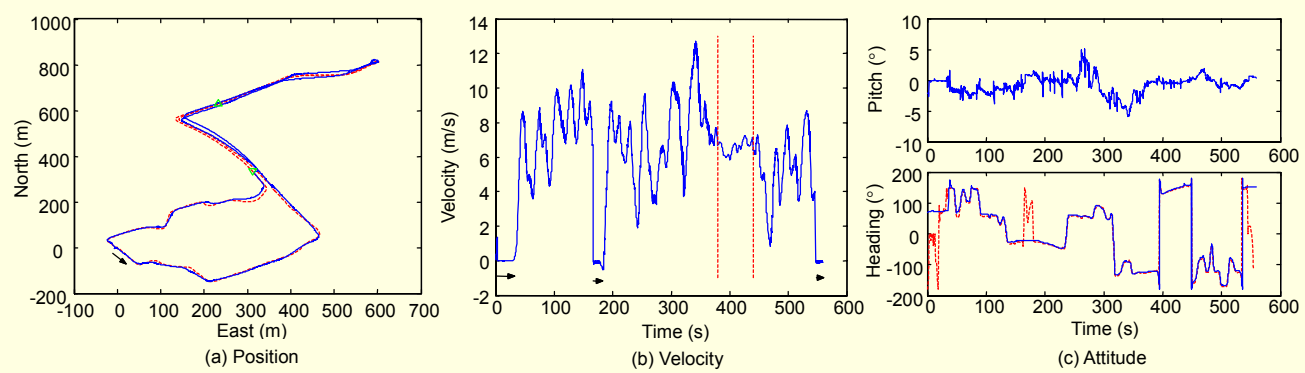

Fig. 14. Results of the DR/GPS using the SPKF (initial estimated heading angle is 70 °).

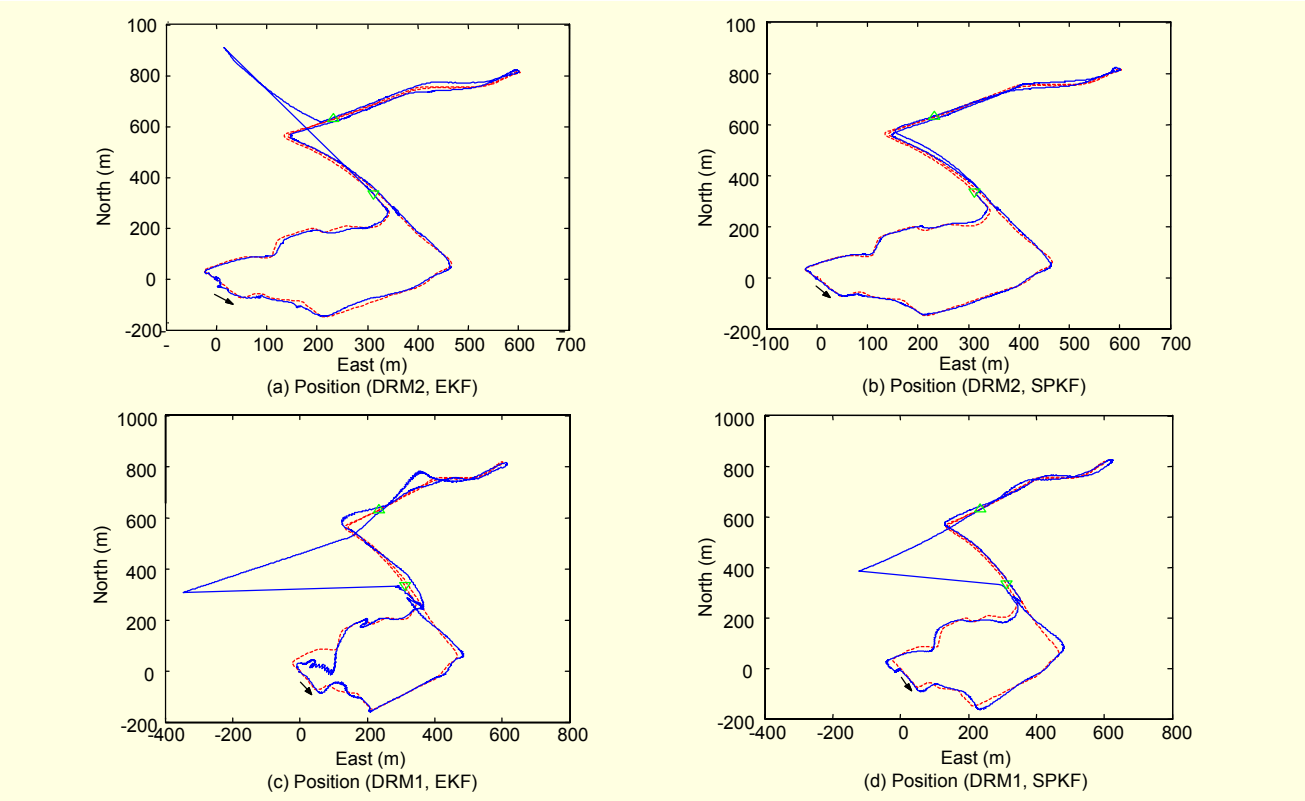

Fig. 15. Results of DR/GPS (initial estimated heading angle is 0 °).

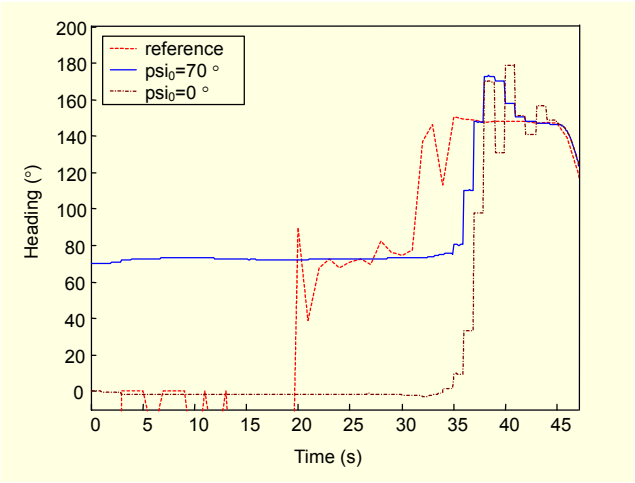

Fig. 16. Results of heading angle estimation using the DRM2 and SPKF.

update. Because the initial heading angle cannot be determined unless a magnetic compass or high-grade gyro module is utilized, the initial heading angle is generally set by 0. Figure 15 shows the results of DR/GPS integration when the initial estimated heading angle is 0. As can be seen in this figure, the SPKF can provide a satisfactory position solution when DRM2 is utilized. In the EKF case, a somewhat large error is generated in the GPS signal blockage. However, the DR scheme restricts the error to within a small amount when a GPS signal is available. When DRM1 is used, however, the EKF provides an unreliable solution because of the erroneous Jacobian matrix. Because the SPKF does not need a Jacobian matrix, a large error can be avoided when a GPS signal is available. Therefore, we can conclude that DRM2 and the DR/GPS system using the SPKF have satisfactory performance.

Figure 16 shows the results of heading angle estimation. In conclusion, the navigation system using low-cost sensors for Telematics can provide a good performance solution if DRM2 and the SPKF are utilized.

V. Conclusions

A DR scheme for low-cost land navigation has been proposed and a DR/GPS system has been designed using the sigma point Kalman filter. These performances have been examined by observability analysis and some simulations under various situations. The presented DR scheme utilizes an accelerometer and two gyros and has a potential robustness to noisy environments. In a stand-alone DR system, this DR scheme does not show an undetectable error that can occur on the curve trajectory in a conventional DR(INS) construction containing low-grade inertial sensors. In a DR/GPS system, a reliable solution can be provided even in the case when the initial heading estimation error is large due to the DR scheme. Moreover, the DR/GPS system using the SPKF has a better performance than that using the EKF. The robustness range to the initial heading estimation error broadens. And a more stable navigational solution can be provided in an urban environment.

The above results show that the fundamental limitation of the stand-alone DR system and the DR/GPS system can be overcome by the presented DR scheme and the SPKF, so that a stable low-cost land navigation system for location-based service can be successfully accomplished.

Appendix

A Jacobian matrix for the EKF is made by deriving the error equation of the state variables. In this work, the error equation is derived using the linear perturbation method.

Position error equation is derived from (5) and (7) as

$$\delta P_k^n = \delta P_{k-1}^n + \begin{bmatrix} \cos\psi_k \\ \sin\psi_k \end{bmatrix} d_k \cdot \delta V_{x,k}^h + V_{x,k}^h d_k \begin{bmatrix} -\sin\psi_k \\ \cos\psi_k \end{bmatrix} \delta\psi_k .$$

The velocity error equation is derived from (4), (6), and (11). First, (4) is perturbed as

$$\begin{aligned} V_{x,k}^h + \delta V_{x,k}^h &= V_{x,k-1}^h + \delta V_{x,k-1}^h \\ &\quad + \left(\left(SF_{ax} + \delta_{ax,k} \right) f_{x,k}^b - g\sin\left(\theta_k + \delta\theta_k\right) \right) \\ &\quad \times \cos\left(\theta_k + \delta\theta_k\right) d_k \\ &\cong V_{x,k-1}^h + \delta V_{x,k-1}^h + \left(SF_{ax} f_{x,k}^b - g\sin\theta_k \right) \cos\theta_k d_k \\ &\quad + f_{x,k}^b \cos\theta_k d_k \cdot \delta_{ax,k} \\ &\quad + \left(g\sin^2\theta_k - SF_{ax} f_{x,k}^b \sin\theta_k - g\cos^2\theta_k \right) d_k \cdot \delta\theta_k . \end{aligned}$$

Therefore, the velocity error equation is written as

$$\begin{aligned} \delta V_{x,k}^h &= \delta V_{x,k-1}^h + \left(SF_{ax} f_{x,k}^b - g\sin\theta_k \right) \cos\theta_k d_k \\ &\quad + f_{x,k}^b \cos\theta_k d_k \cdot \delta_{ax,k} \\ &\quad + \left(g\sin^2\theta_k - SF_{ax} f_{x,k}^b \sin\theta_k - g\cos^2\theta_k \right) d_k \cdot \delta\theta_k . \end{aligned}$$

Pitch error and heading error equations are derived using (12) as follows:

$$\delta\theta_k = \delta\theta_{k-1} + \omega_y^b \cdot \delta_{gy} ,$$

$$\delta\psi_k = \delta\psi_{k-1} + \omega_z^b \cdot \delta_{gz} .$$

Finally, sensor scale factor error equations are modeled as a random constant.

$$\delta_{ax,k} = \delta_{ax,k-1},\ \delta_{ax,0} \sim N(0, P_{ax}) ,$$

$$\delta_{gy,k} = \delta_{gy,k-1},\ \delta_{gy,0} \sim N(0, P_{gy}) ,$$

$$\delta_{gz,k} = \delta_{gz,k-1},\ \delta_{gz,0} \sim N(0, P_{gz}) .$$

References

[1] Seong-Baek Kim, Kyung-Ho Choi, Seung-Yong Lee, Ji-Hoon Choi, Tae-Hyun Hwang, Byung-Tae Jang, and Jong-Hun Lee, "A Bimodal Approach for Land Vehicle Localization," *ETRI Journal*, vol. 26, no. 5, Oct. 2004, pp. 497-500.

[2] W. Abdel-Hamid, T. Abdelazim, N. El-Sheimy, and G. Lachapelle, "Improvement of MEMS-IMU/GPS Performance Using Fuzzy Modeling," *GPS Solution*, vol. 10, no, 2, Feb. 2006, pp. 1-11.

[3] Y. Li, J. Wang, C. Rizos, G. Baitch, and D. Kinlyside, "Application of GPS/INS Integration Technique to Bushfire Monitoring," *Spatial Sciences Conference*, Melbourne, Australia, 12-16, Sept. 2005, pp. 1394-1403.

[4] J.A. Farrel and M. Barth, *The Global Positioning System and Inertial Navigation*, McGraw-Hill, 1999, pp. 246-251.

[5] M.S. Grewal, L.R. Weill, and A.P. Andrews, *Global Positioning Systems, Inertial Navigation, and Integration*, John Wiley & Sons, Inc., 2001, pp. 252-264.

[6] Seong Yun Cho and Chan Gook Park, "A Calibration Technique for a Redundant IMU Containing Low-Grade Inertial Sensors," *ETRI Journal*, vol. 27, no. 4, Aug. 2005, pp. 418-426.

[7] M. Boutayeb, H. Rafaralahy, and M. Darouach, "Convergence Analysis of the Extended Kalman Filter Used as an Observer for Nonlinear Deterministic Discrete-Time Systems," *IEEE Trans. Automatic Control*, vol. 42, no. 4, Apr. 1997, pp. 581-586.

[8] K. Reif, S. Gunther, E. Yaz, and R. Unbehauen, "Stochastic Stability of the Discrete-Time Extended Kalman Filter," *IEEE Trans. Automatic Control*, vol. 44, no. 4, Apr. 1999, pp. 714-728.

[9] S. Julier, J. Uhlmann, and H. Durrant-Whyte, "A New Approach for Filtering Nonlinear Systems," *Proc. Am. Contr. Conf.,* 1995, pp. 1628-1632.

[10] S. Julier, J. Uhlmann, and H. Durrant-Whyte, "A New Method for Nonlinear Transformation of Means and Covariances in Filters and Estimators," *IEEE Trans. Automatic Control*, vol. 45, no. 3, 2000, pp. 477-482.

[11] S. Julier and J. Uhlmann, "Reduced Sigma Point Filters for the Propagation of Means and Covariances Through Nonlinear Transformations," *Proc. Am. Contr. Conf.*, 2002, pp. 887-892.

[12] S. Julier and J. Uhlmann, "The Scaled Unscented Transformation," *Proc. Am. Contr. Conf.*, 2002, pp. 4555-4559.

[13] E. Wan and R. Van der Merwe, "The Unscented Kalman Filter for Nonlinear Estimation," *Proc. IEEE Symposium on Adaptive Systems for Signal Processing Communications and Control*, Oct. 2000, pp. 153-158.

[14] R. Van der Merwe, E. Wan, and S. Julier, "Sigma-Point Kalman Filters for Nonlinear Estimation and Sensor-Fusion – Applications to Integrated Navigation," *Proc. AIAA Guidance, Navigation, and Control Conf. and Exhibit*, 2004.

[15] E.H. Shin and N. El-Sheimy, "An Unscented Kalman Filter for In-Motion Alignment of Low-Cost IMUs," *Proc. IEEE Frames Conf*, 2004, pp. 273-279.

[16] R.M. Rogers, "IMU In-Motion Alignment Without Benefit of Attitude Initialization," *Journal of the Institute of Navigation*, vol. 44, no. 3, Fall 1997, pp. 301-312.

[17] S.Y. Cho and W.S. Choi, "A Robust Positioning Technique in DR/GPS Using the Receding Horizon Sigma Point Kalman FIR Filter," *Proc. IEEE IMTC 2005*, 2005, pp. 1354-1359.

Seong Yun Cho was born in Jinju, Korea, in 1974. He received the BS, MS, and PhD degrees in the Department of Control and Instrumentation Engineering from Kwangwoon University, Korea, in 1998, 2000, and 2004. In 2003, he was with the Automation and System Research Institute (ASRI), Seoul National University, Korea, where he worked on the development of a tilt compensation algorithm for a magnetic compass with Samsung Advanced Institute of Technology (SAIT) as a Research Assistant. In 2004, he was with the School of Mechanical and Aerospace Engineering, Seoul National University, Korea, where he was a postdoctoral fellow, BK21. Since 2004, he has been with Electronics and Telecommunications Research Institute (ETRI), Korea, as a Senior Member of Research Staff. His research interests include navigation systems (INS, INS/GPS, PNS), filter design for linear/nonlinear systems, and Telematics application systems.

Wan Sik Choi was born in Namwon, Korea, in 1954. He received the BS degree in the Department of Mechanical Engineering from Sung Kyun Kwan University, Korea, in 1979 and the MS degrees in mechanical engineering and applied mathematics from The University of Alabama, USA, in 1986 and 1988, respectively. He received the PhD degree in the Department of Mechanical Engineering from The University of Alabama, USA, in 1992. He was with the Agency for Defense Development (ADD), Korea, from 1979 to 1984 as a researcher. Since 1992, he has been with ETRI, Korea, as a Senior/Principal Member of Research Staff. His research interests include telematics, high precision positioning, and stochastic optimal control.